Final Draft

of the original manuscript

Behl, M.; Razzaq, M.; Mazurek-Budzyñska, M.; Lendlein, A.:

Polyetheresterurethane Based Porous Scaffolds with Tailorable Architectures by Supercritical CO2 Foaming.

In: MRS Advances. Vol. 5 (2020) 45, 2317 - 2330.
First published online by Cambridge University Press: 08.09.2020

https://dx.doi.org/10.1557/adv.2020.345

Polyetheresterurethane Based Porous Scaffolds with Tailorable Architectures by Supercritical CO_2 Foaming

Marc Behl[1], Muhammad Yasar Razzaq[1], Magdalena Mazurek-Budzyńska[1], Andreas Lendlein[1,2]*

[1] *Institute of Biomaterial Science, Helmholtz-Zentrum Geesthacht, Kantstr. 55, 14513 Teltow, Germany*
[2] *Institute of Chemistry, University of Potsdam, Karl-Liebknecht-Str. 24-25, 14476 Potsdam, Germany*

*Correspondence to: Prof. Andreas Lendlein
andreas.lendlein@hzg.de

ABSTRACT

Porous three-dimensional (3D) scaffolds are promising treatment options in regenerative medicine. Supercritical and dense-phase fluid technologies provide an attractive alternative to solvent-based scaffold fabrication methods. In this work, we report on the fabrication of poly-etheresterurethane (PPDO-PCL) based porous scaffolds with tailorable pore size, porosity, and pore interconnectivity by using supercritical CO_2 ($scCO_2$) fluid-foaming. The influence of the processing parameters such as soaking time, soaking temperature and depressurization on porosity, pore size, and interconnectivity of the foams were investigated. The average pore diameter could be varied between 100 – 800 µm along with a porosity in the range from (19 ± 3 to 61 ± 6)% and interconnectivity of up to 82%. To demonstrate their applicability as scaffold materials, selected foams were sterilized via ethylene oxide sterilization. They showed negligible cytotoxicity in tests according to DIN EN ISO 10993-5 and 10993-12 using L929 cells. The study demonstrated that the pore size, porosity and the interconnectivity of this multi-phase semicrystalline polymer could be tailored by careful control of the processing parameters during the $scCO_2$ foaming process. In this way, PPDO-PCL scaffolds with high porosity and interconnectivity are potential candidate materials for regenerative treatment options.

INTRODUCTION

Porous 3D scaffolds have tremendous application potential in regenerative therapies, e.g. for the repair of cartilage in patients with osteoarthritis, as they support cell attachment, differentiation, and proliferation to regenerate the tissue. To date, several methods have been reported for the fabrication of 3D scaffolds, some of which include processes such as solvent casting with particulate leaching, compression molding, freeze drying, heat sintering, injection molding, layer-by-layer printing or sintering, and electrospinning. Each of these methods has its own advantages, but these methods typically make use of large amounts of organic solvents and/or exposure to elevated temperatures [1-7]. To overcome this challenge, supercritical carbon dioxide ($scCO_2$) has been used as a foaming agent to form 3D scaffolds. $scCO_2$ being inexpensive, nontoxic, nonflammable, enables a low critical temperature and pressure (T_c = 31.1 °C and P_c = 73.8 bar) and is suitable for foaming of polymeric materials. It reduces the polymer melt viscosity by decreasing the glass transition temperature (T_g) or melting temperature (T_m) due to its high solubility in polymers. Here, the molecular structure and morphology of the polymers plays an important role to determine the solubility of the $scCO_2$ in the polymer. Furthermore, the amount of CO_2 that can be absorbed by the polymer during the soaking step, the viscosity of the swollen polymer, the nucleation density (pore number), and the rate at which $scCO_2$ diffuses from the matrix to the growing pores are all dependent on the

processing parameters, such as temperature, pressure, pressure drop, and depressurisation rate. Therefore, the resulting foam structures can be controlled by manipulating these processing conditions. $scCO_2$ foaming can be performed as an integrated process for loading with small molecules as required by drug release applications [8].

In addition to a suitable pore morphology, the matrix should provide adequate mechanical integrity to support the load-bearing activities of the tissue and should only act as a temporary substitute to enable regeneration. The latter aspect requires materials that are capable of degrading into chemically benign components and should not be harmful to the surrounding cells [9-17]. Several scaffold materials have been investigated for the tissue engineering of bone and cartilage including hydroxyapatite (HA), poly(α-hydroxyesters) such as polylactide (PLA) or polyglycolide (PGA) or their copolymers and naturally occurring polymers such as collagen, hyaluronic acid and chitin. The synthetic polymers are too rigid and their brittleness limits their use for load-bearing tissue regeneration (e.g., cartilage, bone, etc.), and acidic by-products produced during degradation can lead to an inflammatory response in the body. Although naturally occurring polymers show promise here, especially because they promote chondrogenesis and mimic the biochemical properties of cartilage, they are expensive and have poor mechanical properties [18-25]. Recently, poly(p-dioxanone) (PPDO) and poly(ε-caprolactone) (PCL) based constructs have been applied in tissue engineering applications, owing to their flexibility, as well as histocompatibility and low toxicity of their degradation products in vivo, even though their degradation rates are usually too fast or slow for many applications [26]. PPDO loses 50% of its initial strength within 3 weeks, whilst PCL needs 3 years for complete degradation in the body. By blending PPDO and PCL with different p-dioxanone (DO) and ε-caprolactone (CL) ratios or by diblock formation, their degradation rate can be controlled [27-29]. In addition to the control of the degradation rate, multiblock copolymers with PPDO and PCL segments (PPDO-PCL) enabled the creation of elastic materials with deformability, which even could be functionalized with a shape-memory effect [30]. Furthermore, it could be shown that PPDO-PCL could be integrated into soft tissues whereby a connection between the implant and surrounding tissue was obtained, which could be mechanically loaded [31].

Scaffolds with appropriate pore size, porosity and interconnectivity, are vital for the growth of cartilage cells (chrondocytes), as this strongly influences the cell growth, infiltration and nutrient/waste transport. In general, highly porous scaffolds (>90%) are needed to ensure cell delivery and tissue ingrowth [32]. *In vitro* and *in vivo* studies suggested pore sizes and pore interconnections >200 μm. The permeability and interconnectivity of the scaffold are also crucial in determining cell infiltration and successful tissue growth. However, it is challenging to prepare porous scaffolds with defined pore size and ensure interconnectivity of the pores by the $scCO_2$ foaming process [26]. This challenge is even enhanced in the case of semi-crystalline polymers, in which foaming takes place in molten state with a high risk of collapse of the porous structure because of its low viscosity [8, 33].

We hypothesized that different processing parameters during the $scCO_2$ foaming process would enable PPDO-PCL-based scaffolds with tailorable architectures and interconnected pores. Our concept is to vary soaking time (t_{soak}), temperature (T_{soak}), and depressurization rate (dP/dt) to obtain porous scaffolds with controlled average pore size, porosity, and pore interconnectivity.

Owing to the flexibility, biocompatibility and low cytotoxicity of degradation products, PPDO-PCL was used for the fabrication of porous scaffolds. To explore the relationship between foaming parameters and pore morphology, the pore size, pore size distribution, porosity and interconnectivity were analyzed by SEM and μ-CT. In initial indirect cytotoxicity measurement of the obtained scaffolds a potential cytotoxic influence of the scCO2 foaming process was studied.

EXPERIMENTAL

Materials

Poly(ε-caprolactone) diol, (PCL, trade name CAPA2205, M_n = 2000 g·mol^{-1} Solvay, Warringthon, UK. *p*-Dioxanone (PDO, purity >99%) was purchased from Daiwa Kasei Ind., Japan. 1,8-Octane diol (purity >98%) was provided by Fluka, Taufkirchen, Germany. Dimethyl carbonate (DMC, purity 99%) was obtained from Acros Organics, Geel, Belgium, the ethyl alcohol (purity >95%) was purchased from Berkel AHK, Berlin, Germany and the liquid nitrogen was provided by Linde AG, Germany. Aluminum isopropoxide (AliOPr) (purity >98%) and dibutyltin dilaurate (purity 95%) were from Sigma-Aldrich, Darmstadt, Germany. Lysine diisocyanate (purity 97.8%) was purchased from Chemos GmbH, Regenstauf, Germany.

Synthesis of poly(p-dioxanone) diol (PPDO)

The synthesis of PPDO was carried out according to the procedure described in [34]. In brief, in a dried 1 dm^3 Schlenk flask, 800 g (7.840 mol) of PDO was added, evacuated, kept under nitrogen atmosphere and stirred at 60 °C in an oil bath. 23.397 g (0.160 mol) of 1,8-octanediol and 186.7 mg (0.9 mmol) of AliOPr were added. When the reaction mixture became homogenous, the temperature of the oil bath was raised to 108 °C. After 7 days, the mixture was cooled to 75 °C and dissolved in 2000 ml of dimethyl carbonate under vigorous stirring. Afterwards, 1200 ml of ethanol was added at room temperature under stirring, and then the mixture was rapidly cooled to -12 °C. After 24 hours, the precipitant was decanted, fritted, washed with 4000 ml of ethanol, and dried in the vacuum oven for 14 days at room temperature (yield 66 wt%). The M_n, as determined by multidetector GPC was (3.700 ± 300) g·mol^{-1}.

Synthesis of PPDO-PCL (50/50 mol.%)

The synthesis of PPDO-PCL was carried out in a similar way to the procedure described in [35] with the exception that LDI was used. In a 4000 ml mixing reactor, 500 g (152.4 mmol) of PPDO, 500 g (250 mmol) PCL, 104.809 g (0.495 mol, 92.916 ml) of LDI, and 159.6 mg (149.8 µl) of DBSnDL were dissolved in 2.5 L DMC and reacted at 85 °C for 7 days under nitrogen atmosphere and vigorous stirring. Afterwards, 1.0 g (7 mmol) of 1,8-octanediol was added to react with residual isocyanate groups. The PCL-PPDO was obtained by precipitation in liquid nitrogen and subsequent drying under vacuum until constant weight was achieved (yield 99 wt%). The M_n determined by multidetector GPC was 41.900 ± 700 g·mol^{-1}.

Foaming procedure

The foaming system consisted of the following components: a 600 ml stainless steel, high-pressure autoclave series 28096 (Parr Instrument Company, Moline, USA), a multi-channel process and program controller Imago 500 (JUMO GmbH & Co. KG, Fulda, Germany), two laboratory valves Kämmer Series 185000 (Flowserve Essen GmbH, Essen, Germany), a thermostat PROLINE RP845 (Lauda Dr. R. Wobser GmbH & Co. KG , Lauda-Königshofen, Germany), and a water recirculator Thermo Haake WKL 26 (Haake Technik GmbH, Vreden, Germany). A pneumatic-pump K-1900 (KNAUER Wissenschaftliche Geräte GmbH, Berlin, Germany) was used to charge CO_2 into the autoclave. A homemade LabVIEW 8.2.1 (National Instruments, Germany) program enabled the control of the process used during the foaming procedure as well as of the depressurization rate by controlling the laboratory valves, which were connected to outflows of different flow rates.

The foaming process was performed as follows: three dried cylindrical glass vials (20 mm diameter and 50 mm height) containing 2.5 g of dried PPDO-PCL each were placed in an autoclave, which was heated to the intended soaking temperature (T_{soak} = 100 °C), and filled with CO_2 at 150 bar. The system was maintained at a constant temperature (T_{soak}) and pressure over a defined time period (soaking time, t_{soak}). The soaking time period was followed by a depressurization of the $scCO_2$, during which the pressure was decreased to ambient pressure with a controlled depressurization rate (dP/dt). Here, the temperature was kept constant at T_{soak}, or was lowered at a controlled cooling rate (dT/dt). Afterwards, the vials containing the foamed sample were removed from the autoclave.

Characterization techniques

^{1}H NMR spectra were acquired on a 500 MHz spectrometer (DRX 500 Avance, Bruker, Rheinstetten, Germany) at room temperature using tetramethylsilane as an internal reference and $CDCl_3$ as solvent, and were analyzed with MestReNovav.6.2.0-7238 (Mestrelab Research S.L) software. The error of the method was estimated based on the error of the integral peak area (around 5%).

Multidetector GPC measurements were performed at a solvent flow rate of 1 $mL \cdot min^{-1}$ at 35 °C using chloroform as eluent and 0.2 wt% toluene as an internal standard. The system was equipped with a pre-column, two 300 mm x 8.0 mm linear GRAM columns (Polymer Standards Service GmbH [PSS], Mainz, Germany), an isocratic pump (PU-2080), an automatic injector AS 2050 (both Jasco, Tokyo, Japan), a refractive index detector (Shodex RI-101, Munich, Germany), and a differential viscometer (WGE n-100x/n-200x,WGE Dr Bures GmbH, Dallgow-Doeberitz, Germany). The SEC software WINGPC UniChrom (PSS) was used to determine the molecular weight distributions by universal calibration with polystyrene standards from 1.82 KD till 975 KD (PSS). The error of the measurement method was estimated as 10% based on measurements of polystyrene standards.

Differential Scanning Calorimetry (DSC) measurements were performed on a DSC 204 Phoenix (Netzsch, Selb, Germany) with a constant heating and cooling rate of 5 $K \cdot min^{-1}$. Whenever the maximum or minimum temperature in the testing program was reached, the temperature was kept constant for 2 min. Samples were investigated in a temperature range between -100 and 100 °C in three cycles: heating from room temperature to 250 °C, then cooling to -100 °C and again heating to 100 °C.

Scanning electron microscope pictures were performed with a desktop-SEM Phenom G2 from Phenom World (LOT-Oriel Group Europe, Darmstadt, Germany).

The cellular structures, pores size, volume pore size distribution and pore interconnectivity were determined by a micro-computed tomography (μCT) instrument (Procon X-ray GmbH, Sarstedt, Germany) with a L9181-02 X-ray source (Hamamatsu Photonics K.K., Hamamatsu, Japan) and a C7942SK-05 detector (Hamamatsu Photonics K.K., Hamamatsu, Japan). Recording of grey shadow images was carried out at 40 kV and 0.2 mA (integration time = 750 ms; averaging of images was 6). The selected magnification resulted in a voxel edge length of 6.7 to 9.1 microns dependent on the pore size of the sample. The grayscale image was taken at 0.45 grd angular distance.

3D-images were reconstructed by using the software Volex (Fraunhofer EZRT, Germany). The 3D reconstructions were evaluated with the software MAVI (Fraunhofer ITMW, Germany), in which the binarization according to Otsu and the segmentation was done using the pre-flooded watershed model. To mitigate extreme values, a binomial filter was used before the calculations. The porosity of the samples corresponds to the volume ratio of the polymer, accessible after binarization, to the total volume of the tested sample. The surface analysis after segmentation of the 3D reconstruction was done with the software Meshmixer (Autodesk Inc., US). The interconnectivity was calculated from the volume ratio of these categories.

Cytotoxicity evaluation was adapted from the procedure described in reference [36]. 5 mL of phosphate buffered saline (without magnesium and calcium) (PBS) was added for the wetting of the porous polymer sample. After 5 minutes of incubation, the PBS solution was removed. The polymer samples were immediately transferred into a new Falcon tube (15 mL) and weighed. According to DIN EN ISO 10993-12, 1 mL of eluate medium was added to 0.1 g of polymer sample for extraction.

If not mentioned otherwise, the errors of the measurements were calculated based on the average value of results of three samples. The standard deviations (σ) were calculated based on equation 1, where $\bar{x}$ is the average value of all results and n is number of samples.

$$\sigma = \sqrt{\frac{\Sigma(x-\bar{x})^2}{n}} \qquad (1)$$

RESULTS AND DISCUSSION

Multiblock copolymers (PPDO-PCL) have been synthesized in a polyaddition reaction from PPDO, PCL, and LDI and were purified by precipitation from the reaction mixture. A molecular weight of M_n = (41,900 ± 700) g·mol^{-1} and a polydispersity index (PDI) = 1.75 were determined by GPC. A PPDO content of (54 ± 3) wt% was verified by ^{1}H NMR. Fig. 1 displays the GPC curve and ^{1}H-NMR spectrum as well as its assignment.

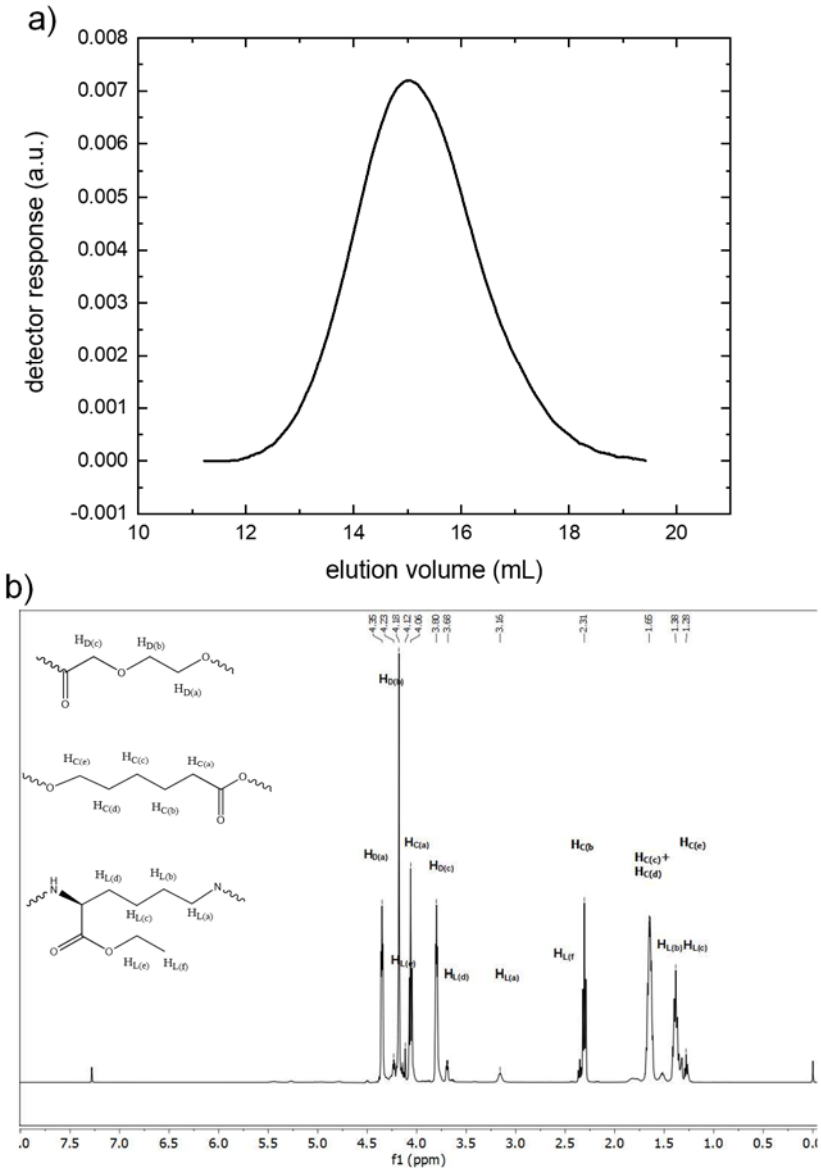

Figure 1. Characterization of PPDO.-PCL a) Gel permeation elugram of PPDO-PCL in chloroform. B) ^{1}H NMR of PPDO-PCL in $CDCl_3$ and assignment of signals.

The structural formula is shown in Fig. 2a. Thermal properties of the multi-block PDDO-PCL copolymer were determined by DSC to select appropriate temperature regimes for foaming related to the melting transition of crystalline domains. The DSC thermogram in Fig. 2b indicated two melting transition areas corresponding to the melting of PCL and PPDO domains with $T_{m,PCL}$ = (21 ± 2 - 42 ± 2) °C and $T_{m,PPDO}$ = (70 ± 2 - 94 ± 2) °C and the maxima at $T_{m\_max,PCL}$ = (32 ± 2) °C and $T_{m\_max,PPDO}$ = (85 ± 2) °C. The melting of the PCL domains seems to be superimposed by a second glass transition, which is higher

than the T_gs associated the domains of the single blocks ($T_{g,PCL}$~ -60 °C, $T_{g,PPDO}$ ~ -5 °C) can be attributed to a mixed phase from the PCL, PPDO and the urethane bonds.

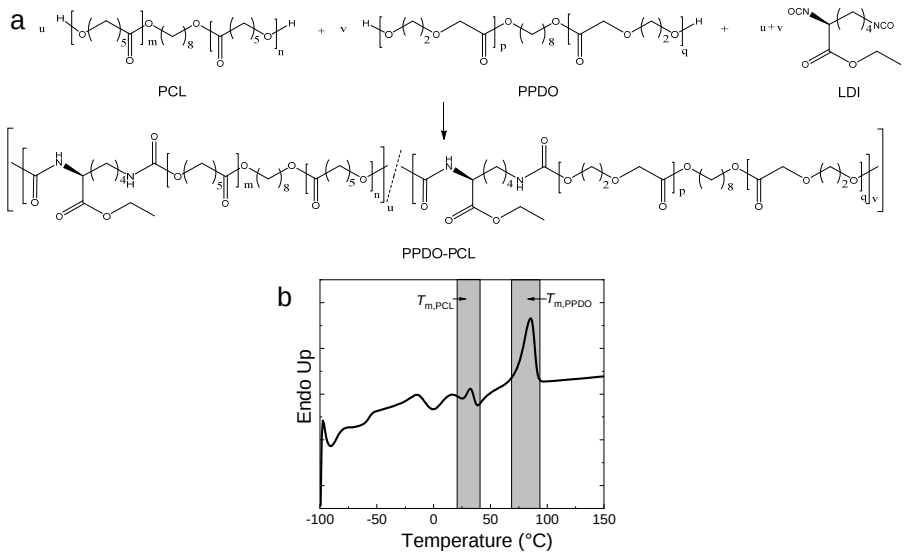

Figure 2. a) Reaction scheme and structural formula of the PPDO-PCL used for scaffold fabrication, b) DSC thermogram of the bulk PPDO-PCL.

To explore the effect of temperature on foaming of the PPDO-PCL, the temperature was varied between 75 °C and 95 °C, while the pressure, soaking time and depressurization rate were kept constant at 140 MPa, 60 min, and 8 bar·min^{-1} respectively. At T_{soak} = 75 °C, which is below the melting temperature (T_m = (85 ± 1) °C) of the polymer, foaming was not observed, which is in contrast to the foaming of PCL in which foaming was observed below $T_{m,PCL}$ [37]. At T_{soak} = 75 °C, the polymer was not molten and the crystalline domains prevented the $scCO_2$ from penetrating into the polymer even after soaking time periods of 150 min. When T_{soak} was raised to 85 °C (Fig. 3b), highly dense polymer foams with a mean pore diameter of (50 ± 10) µm were attained. At this temperature, a partial melting of the crystalline PPDO domains enabled a restricted diffusion of the $scCO_2$ into the polymer and a limited increase of free volume. A further increase of the temperature to T_{soak} = 95 °C resulted in foams with larger pores and a mean pore diameter of (150 ± 32) µm (Fig. 3a). At this temperature, above $T_{m,PPDO}$, the crystalline domains were completely molten, which facilitated the mobility of the polymer chains and higher diffusivity of the $scCO_2$ into the melt phase [33]. These experiments showed that a temperature either in the melting range or higher than $T_{m,PPDO}$ could be used to tailor the pore size of the resulting foam.

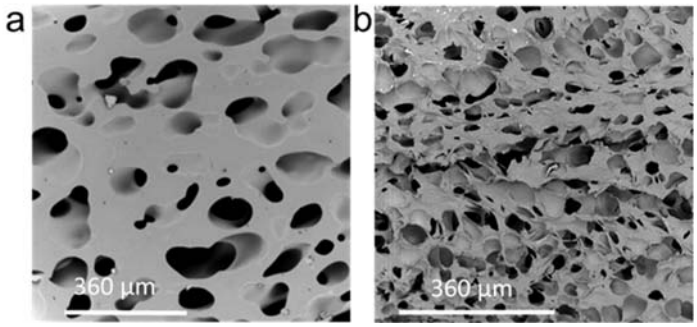

Figure 3: SEM images showing the influence of soaking temperature on foam morphology. The soaking time (90 min) and depressurization rate of 8 bar·min^{-1} were kept constant. a) T_{soak} = 95 °C min, b) T_{soak} = 85 °C.

The influence of soaking time (t_{soak}) period on scaffold morphology was explored in experiments with t_{soak} = 30, 60, 90, 120 and 150 min while the temperature and pressure were kept constant at 95 °C (> $T_{m,PDDO}$) and 140 bar. The depressurization rate dp/dt was also kept constant at 8 bar·min^{-1}. The influence of t_{soak} was investigated by SEM and 3D µ-CT (Fig. 4). Using software-based surface analysis after segmentation of the 3D reconstruction it was possible to distinguish between pores that are in contact with each other from those that are isolated.

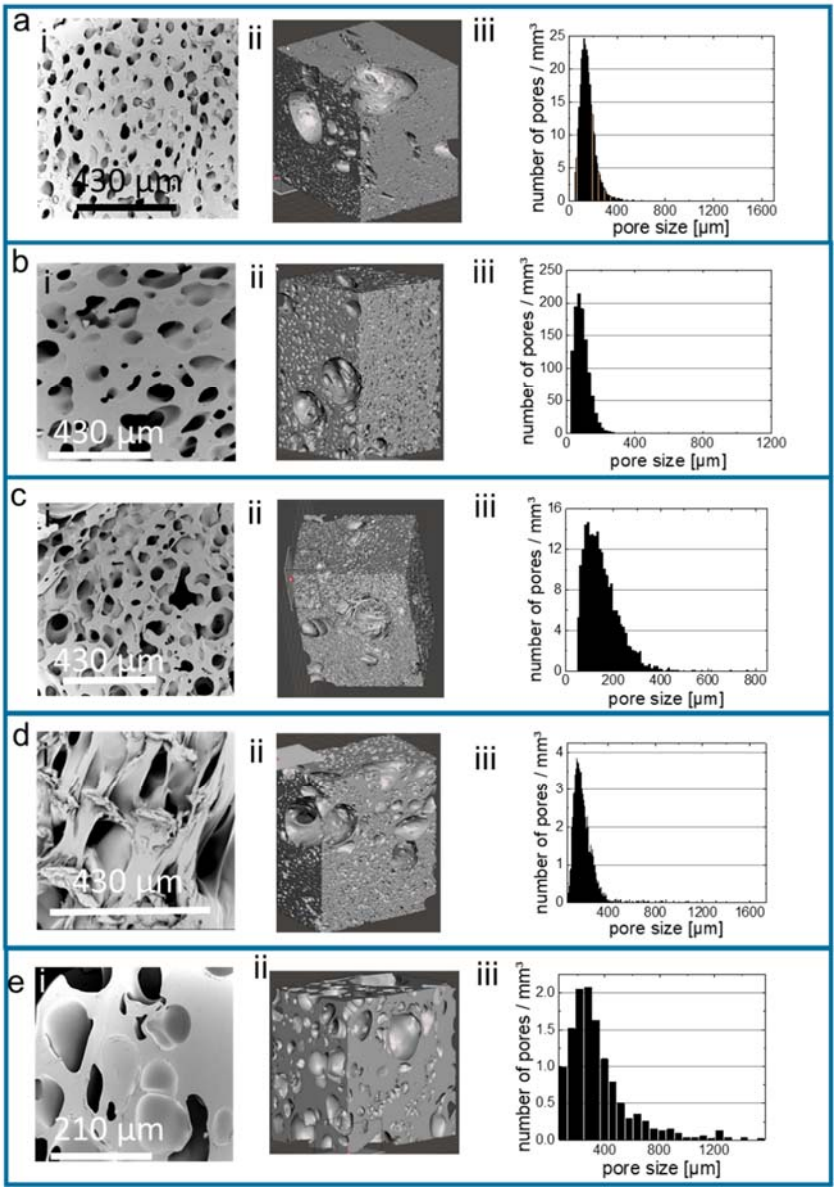

Figure 4. i) SEM, ii) 3D µ-CT images and iii) pore size distribution of the scaffolds prepared with different soaking times a) 30 min b) 60 min c) 90 min d) 120 min e) 150 min. The other processing parameters were kept constant for all samples.

The foam structure of PPDO-PCL can be described as non-uniform with predominantly small pores and occasionally some large pores. The mean pore diameter of the scaffolds decreased from (155 ± 10) µm at t_{soak} = 30 min to (90 ± 20) µm at t_{soak} = 90 min. The soaking time correlates to the amount of $scCO_2$ absorbed in the polymer. The higher the concentration of $scCO_2$ dispersed in the polymer, the higher the density of nucleation sites generated during the depressurization stage, which results in scaffolds with

smaller pores. The relationship of the nucleation rate and the concentration of the CO_2 can be described by the equation (2) according to reference [38].

$$N_{homo}^{0} = C_0 f_0 exp\left(\frac{-16\pi\gamma^3}{3\,\Delta P^2 \cdot kT}\right) \quad (2)$$

N_{homo}^{0} is the number of nuclei generated per cm^3 per second, C_o is the concentration of the gas (number of molecules per cm^3), f_o is the frequency factor of the gas molecules, k is Boltzmann's constant, T is absolute temperature, ΔP is magnitude of the quench pressure and γ is the surface energy of the bubble interface. Nevertheless, further increase of t_{soak} resulted in an increase of the mean pore diameter to (179 ± 31) µm (t_{soak} = 120 min) and (359 ± 20) µm (t_{soak} = 150 min), which could be attributed to the saturation of the polymer by $scCO_2$. This larger mean pore diameter could support cell growth and result in a larger cell size [26]. This increase in mean diameter could be related to the solidification of the PPDO-PCL matrix, which could be too slow for the higher amount of $scCO_2$ with raised soaking times and corresponds with a decrease in the number of pores per mm^2.

To further explore the effect of t_{soak}, scaffolds were synthesized with depressurization rates of dp/dt = 6 bar·min^{-1} and 4 bar·min^{-1}. Here, similar variations of mean pore size diameters were observed when the t_{soak} was increased from 30 min to 150 min whereas the porosity was always higher than 40% (Figure 5).

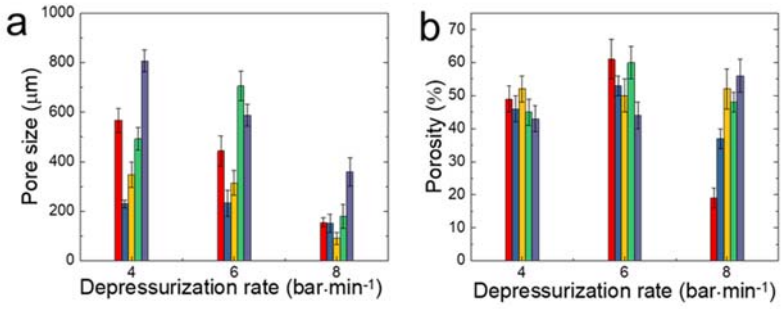

Figure 5: Effect of varied depressurization rate and soaking time on the pore size (a) and percentage porosity (b) of the scaffolds. t_{soak} = 30 min (red column), t_{soak} = 60 min (light blue column), t_{soak} = 90 min (yellow column), t_{soak} = 120 min (green column) and t_{soak} = 150 min (blue column).

Furthermore, depressurization rate affected foam morphology tremendously. The effect of depressurization rate on the pore size and pore size distribution is shown by SEM and µ-CT results in Figure 6. By increasing the depressurization rate from 4 bar·min^{-1} to 8 bar·min^{-1} while the other parameters of temperature, pressure and soaking time were kept constant at 95 °C, 140 MPa and 30 min, pore sizes of the scaffolds significantly decreased from (567 ± 104) µm (4 bar·min^{-1}) to (155 ± 35) µm (8 bar·min^{-1}).

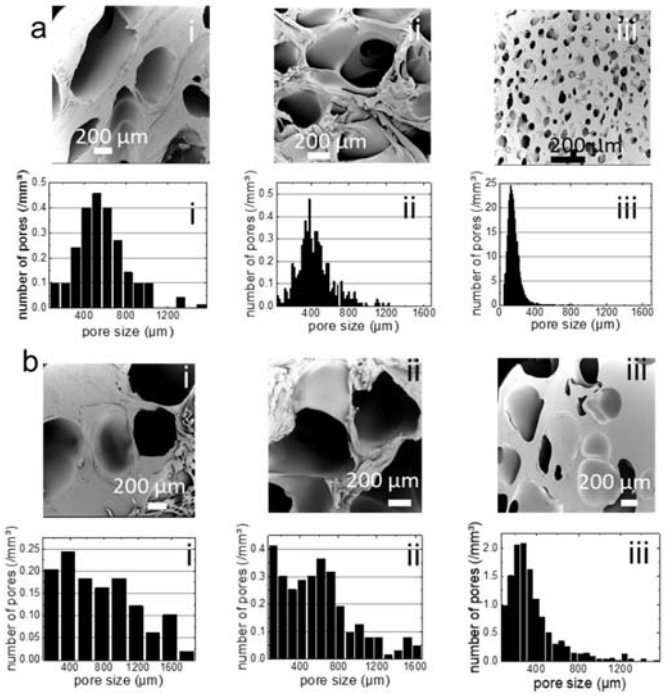

Figure 6: SEM images and pore size distribution of the foams prepared with soaking time periods of a) 30 min and b) 150 min under variation of depressurization rates with i) 4 bar·min^{-1} ii) 6 bar·min^{-1} iii) 8 bar·min^{-1}.

Pore size distribution became broader when the depressurization rate was decreased. Fast depressurization led to higher level of supersaturation of $scCO_2$, facilitating nucleation and resulting in smaller pores [26, 33]. In addition, the fast nucleation and quenching of $scCO_2$ restricted the pore growth, which resulted in more homogeneous foams. When the pressure difference between bubbles and system was small, a low depressurization rate results in fewer nucleation sites but abundant time for pore growth and coalescence as more CO_2 was available for expansion of pores than for nucleation. A similar finding was observed for foaming of PCL only [39]. For those pores formed at the beginning of the pressure quench more CO_2 was available and they had more time to grow, while the pores formed at a later stage of the pressure quench had only a limited time period available until solidification of the matrix occurred, thus they are widening the distribution of pore sizes. In addition to the process of bubble formation, also the decrease of the melting temperatures of the PPDO-PCL domains by the $scCO_2$ caused by the vapor pressure reduction, the reduction of the PPDO-PCL domains by the formation of smaller domain sizes as well as influence of $scCO_2$ on the phase separation by acting as a homogenizer needs to be considered [37]. Tailoring of depressurization rate or soaking time resulted in scaffolds with interconnected morphology and the percentage of interconnected pores ranged between (19 ± 3)% and (61 ± 6)%.

Suitability of the scaffold materials for further biofunctionality testing was demonstrated in cytotoxicity tests according to DIN EN ISO 10993-5 and 10993-12 using L929 fibroblast. In the lactase dehydrogenase (LDH) release and mitochondrial activity tests all samples displayed negligible cytotoxicity. Cytotoxicity levels of 1 or below were determined when compared to the control with $p > 0.05$ (Fig. 7c, d). Scale: a level of

difference ≤ 5% : cytotoxicity levels = 0, level of difference ≤ 25% : cytotoxicity levels = 1, level of difference between 25% and 50% : cytotoxicity levels = 2, level of difference between 50% and 75% : cytotoxicity levels = 3, level of difference > 75% : cytotoxicity levels = 4. In addition, a negligible change in the morphology of the cells compared to the negative control was observed as shown in Fig. 7a, b. This change was also observed in the bulk material before processing by $scCO_2$ foaming. In this way, it could be demonstrated that the scCO2 processing did not result in the scaffolds having a cytotoxic effect. As the beneficial interaction of the bulk material with tissue was already demonstrated [35], these scaffolds could be promising candidate materials for applications in regeneration like cartilage tissue.

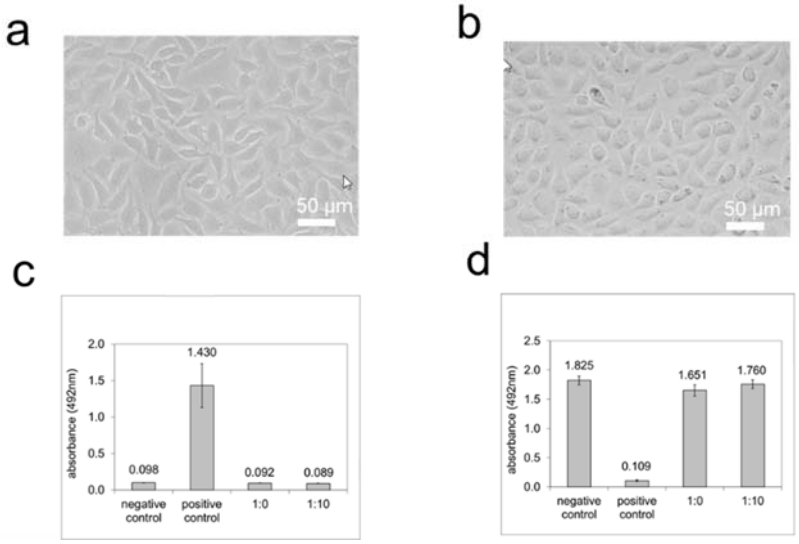

Figure 7: Representative results from cytotoxicity analysis of a PPDO-PCL scaffold a) Negative control, b) sample extract, c) LDH release, d) mitrochondrial activity. Values are given as arithmetic mean (bar) ± standard deviation (lines perpendicular to bar), number of experiments, n = 8.

CONCLUSIONS

Polyetheresterurethane (PPDO-PCL) based porous scaffolds with tailorable pore size, porosity, and pore interconnectivity could be created by $scCO_2$ fluid-foaming. Foaming with sufficiently large and interconnected pores could only be achieved if foaming temperature exceeded $T_{m,PPDO}$. Increase of the soaking time resulted between t_{soak} = 30 min to t_{soak} = 90 min resulted in a decrease of pore size from 155 ± 10 µm to (90 ± 20) µm whereas further increase of t_{soak} caused an increase of the pore sizes again to (359 ± 20) µm for t_{soak} = 150 min, which was attributed to saturation by $scCO_2$. However, the significant parameter to control the pore size was the depressurization rate, whereby pore sizes could be decreased from (567 ± 104) µm at 4 bar·min^{-1} to (155 ± 35) µm at 8 bar·min^{-1}. Cytotoxicity tests using L929 fibroblast suggested these scaffolds to be promising candidate materials for further biofunctionality testing.

ACKNOWLEDGEMENT

The authors are thankful for M. Zierke for synthesis, T. Weigel and M. Rettschlag for □-CT imaging and porosity analysis, and A. Ritschel for cytotoxicity testing. This work was financially supported by the Helmholtz Association through programme-oriented funding, and by the Ministry for Science, Research and Cultural Affairs of Brandenburg through the grant of the joint project "Konsequenzen der altersassoziierten Zell- und Organfunktionen" of the Gesundheitscampus Brandenburg (Grant No. GeCa: H228-05/002/008).

REFERENCES

1. X. W. Cao, Y. H. Qiao, Y. X. Chen, G. J. He and H. Lin, *Polym Eng Sci* **56** (9), 980-986 (2016).
2. V. Dolomanova, V. Kumar, R. Pyrz, L. A. O. Madaleno, L. R. Jensen and J. C. M. Rauhe, *Cell Polym* **31** (3), 125-143 (2012).
3. V. Dolomanova, V. Kumar, R. Pyrz, L. A. O. Madaleno, L. R. Jensen and J. C. M. Rauhe, *Cell Polym* **32** (1), 1-19 (2013).
4. T. Ellingham, L. Duddleston and L. S. Turng, *Polymer* **117**, 132-139 (2017).
5. X. Q. Lan, W. T. Zhai and W. G. Zheng, *Ind Eng Chem Res* **52** (16), 5655-5665 (2013).
6. X. X. Wang, V. Kumar and W. Li, *Cell Polym* **31** (1), 1-18 (2012).
7. T. Weigel, G. Schinkel and A. Lendlein, *Expert Rev Med Devic* **3** (6), 835-851 (2006).
8. K. Luetzow, F. Klein, T. Weigel, R. Apostel, A. Weiss and A. Lendlein, *J Biomech* **40**, S80-S88 (2007).
9. N. Goonoo, A. Bhaw-Luximon, G. L. Bowlin and D. Jhurry, *Polym Int* **62** (4), 523-533 (2013).
10. M. Grunlan, D. W. Zhang, M. Hahn, J. Erndt-Marino and A. Jimenez-Vergara, *Abstr Pap Am Chem S* **252** (2016).
11. J. Heitz, C. Plamadeala, M. Wiesbauer, P. Freudenthaler, R. Wollhofen, J. Jacak, T. A. Klar, B. Magnus, D. Kostner, A. Weth, W. Baumgartner and R. Marksteiner, *J Biomed Mater Res A* **105** (3), 891-899 (2017).
12. Y. H. Hu, S. R. Winn, I. Krajbich and J. O. Hollinger, *J Biomed Mater Res A* **64a** (3), 583-590 (2003).
13. N. Iwasaki, Y. Kasahara, S. Yamane, T. Igarashi, A. Minami and S. Nisimura, *Polymers-Basel* **3** (1), 100-113 (2011).
14. A. Jaramillo-Botero, M. Blanco, Y. Y. Li, G. McGuinness and W. A. Goddard, *J Comput Theor Nanos* **7** (7), 1238-1256 (2010).
15. G. Y. Ji, W. T. Zhai, D. P. Lin, Q. Ren, W. G. Zheng and D. W. Jung, *Ind Eng Chem Res* **52** (19), 6390-6398 (2013).
16. G. Z. Jin, T. H. Kim, J. H. Kim, J. E. Won, S. Y. Yoo, S. J. Choi, J. K. Hyun and H. W. Kim, *J Biomed Mater Res A* **101** (5), 1283-1291 (2013).
17. Y. M. Ju, K. Park, J. S. Son, J. J. Kim, J. W. Rhie and D. K. Han, *J Biomed Mater Res B* **85b** (1), 252-260 (2008).
18. H. Y. Mi, S. Palumbo, X. Jing, L. S. Turng, W. J. Li and X. F. Peng, *J Biomed Mater Res B* **102** (7), 1434-1444 (2014).
19. A. V. Nawaby, A. A. Farah, X. Liao, W. J. Pietro and M. Day, *Biomacromolecules* **6** (5), 2458-2461 (2005).
20. G. Pertici, F. Carinci, G. Carusi, D. Epistatus, T. Villa, F. Crivelli, F. Rossi and G. Perale, *J Biol Reg Homeos Ag* **29** (3), 136-148 (2015).
21. M. M. Rahman, M. Shahruzzaman, M. S. Islam, M. N. Khan and P. Haque, *J Polym Eng* **39** (2), 134-142 (2019).
22. P. Ros-Tarraga, A. Murciano, P. Mazon, S. A. Gehrke and P. N. De Aza, *Ceram Int* **43** (8), 6548-6553 (2017).
23. K. B. Ryan and D. J. Mooney, *Tissue Eng Pt A* **21**, S108-S109 (2015).
24. A. Sadiasa, T. H. Nguyen and B. T. Lee, *J Biomat Sci-Polym E* **25** (2), 150-167 (2014).
25. J. San Roman, M. Martin, L. Rojo, R. Rosales and S. Deb, *Tissue Eng Pt A* **21**, S59-S59 (2015).
26. C. Gualandi, L. J. White, L. Chen, R. A. Gross, K. M. Shakesheff, S. M. Howdle and M. Scandola, *Acta Biomaterialia* **6** (1), 130-136 (2010).
27. J. Albuerne, L. Marquez, A. J. Müller, J.-M. Raquez, P. Degée and P. Dubois, *Macromolecular Chemistry and Physics* **206** (9), 903-914 (2005).
28. Y. Brito, M. A. Sabino, G. Ronca and A. J. Müller, *Journal of Applied Polymer Science* **110** (6), 3848-3858 (2008).
29. I. A. Chaim, M. A. Sabino, M. Mendt, A. J. Müller and D. Ajami, *Journal of Tissue Engineering and Regenerative Medicine* **6** (4), 272-279 (2012).
30. A. Lendlein and R. Langer, *Science* **296** (5573), 1673-1676 (2002).

31. D. Rickert, M. O. Scheithauer, S. Coskun, S. Kelch, A. Lendlein and R. P. Franke, *Clin Hemorheol Micro* **36** (4), 301-311 (2007).
32. L. J. White, V. Hutter, H. Tai, S. M. Howdle and K. M. Shakesheff, *Acta Biomaterialia* **8** (1), 61-71 (2012).
33. C. X. Chen, Q. Q. Liu, X. Xin, Y. X. Guan and S. J. Yao, *J Supercrit Fluid* **117**, 279-288 (2016).
34. M. Behl, U. Ridder, Y. Feng, S. Kelch and A. Lendlein, *Soft Matter* **5** (3), 676-684 (2009).
35. B. Hiebl, R. Fuhrmann, F. Jung, K. Kratz, A. Lendlein and R. P. Franke, *Clin Hemorheol Micro* **45** (2-4), 117-122 (2010).
36. J. Cui, K. Kratz, B. Hiebl, F. Jung and A. Lendlein, *Tissue Eng Pt A* **17** (3-4), 563-563 (2011).
37. M. Karimi, M. Heuchel, T. Weigel, M. Schossig, D. Hofmann and A. Lendlein, *J Supercrit Fluid* **61**, 175-190 (2012).
38. S. K. Goel and E. J. Beckman, *Polym Eng Sci* **34** (14), 1137-1147 (1994).
39. M. A. Fanovich and P. Jaeger, *Mat Sci Eng C-Mater* **32** (4), 961-968 (2012).